A NOVEL CAD SYSTEM FOR LOCAL AND GLOBAL EARLY DIAGNOSIS OF ALZHEIMER'S DISEASE BASED ON PIB-PET SCANS

Fatma El-Zahraa A. El-Gamal[1, 2], Mohammed M. Elmogy[1, 2], Mohammed Ghazal[2, 3], Ahmed Atwan[1], Gregory N. Barnes[3], Manuel F. Casanova [4], R. Keynton [5], Ayman S. El-Baz[2]

[1]Information Technology Dept., Faculty of Computers and Information, Mansoura University, Egypt
[2]BioImaging Laboratory, Bioengineering Dept., University of Louisville, Louisville, KY, USA
[3]Dept. of Electrical and Computer Engineering, Abu Dhabi University, UAE
[4]School of Medicine, University of South Carolina, Greenville, South Carolina, USA
[5]Dept. of Neurology, University of Louisville, Louisville, KY, USA
[6]Bioengineering Dept., University of Louisville, Louisville KY, USA

ABSTRACT

This manuscript presents a Computer Aided Diagnosis (CAD) system to assist in the early diagnosis of Alzheimer's disease (AD) with the ability to provide a personalized diagnosis by visualizing the detected abnormality per brain regions (AAL atlas). The CAD system utilizes PiB-PET scans and consists of the following four essential stages- (1) a preprocessing step performs data re-orientation, co-registration, and spatial normalization; (2) partitioning the brain into 116 labeled regions utilizing a brain atlas to facilitate local diagnosis; (3) extraction of features within each region using scale-invariant Laplacian of Gaussian (LoG) that detects the maximum or minimum of a radially symmetric intensity distribution; and (4) construction of two diagnosis layers (local and global) using a Support Vector Machine (SVM) classifier and its probabilistic variant (pSVM). The CAD system was tested on 84 PiB-PET scans (19 normal control (NC) and 65 mild cognitive impairment (MCI)) from the Alzheimer's Disease Neuroimaging Initiative (ADNI) database. The proposed system had a classification accuracy, sensitivity, and specificity of 100%.

Index Terms— Alzheimer's Disease (AD), Early diagnosis, CAD, PIB-PET

1. INTRODUCTION

Alzheimer's disease (AD) is one of the neurodegenerative diseases that targets the central nervous system (CNS). AD represents approximately 70% of dementia cases [1, 2]. AD prevalence increases with age [2, 3], with a 42% prevalence in individuals over 85 years and 6% prevalence between 70 and 74 years old.

AD is a progressive disease that is classified based on severity as early (mild), intermediate (moderate), and late (severe) AD [4]. Early diagnosis of AD can enable clinicians to intervene with therapies to slow disease progression and prolong life [5]. Early diagnosis of AD is challenging as the onset of the pathological changes precedes the onset of clinical symptoms by approximately 10-15 years. During this 10-15 year period, significant neural degeneration may have already occurred. Further, there is a significant intra-patient variability in the clinical and the pathological features [6].

Early diagnosis of AD that utilizes imaging modalities and extract the common features in various diagnostic tests of AD have been reported in literature. Jack et al. [7] presented the role of different AD biomarkers and their relation to disease's progression. The study illustrated that brain-related β-amyloidosis biomarkers (i.e., Positron Emission Tomography (PET) amyloid imaging and cerebrospinal fluid (CSF) amyloid beta $(A\beta)^{42}$) helped in revealing the abnormalities that were identified to occur at the early disease's stages (Aβ abnormalities). The neurodegenerative biomarkers (i.e., CSF tau, structural magnetic resonance imaging (sMRI), and 2-[18F] fluoro-2-deoxy-d-glucose (FDG)-PET), and cognitive symptoms and clinical symptom severity, showed the abnormalities that manifested later in the disease progression.

Despite its role as an early identifier of AD, the clinical utilization of PET-amyloid imaging should be carefully considered as normal, elderly patients may also have elevated Aβ levels. Fortunately, carbon-11 labeled Pittsburgh compound B (^{11}C PiB) has emerged as a promising biomarker for early diagnosis of AD [8,9]. Illán et al. [9] proposed an automatic classification system through utilizing principal component analysis (PCA) and support vector machines (SVM) and compared the influence of the proposed system on the PiB and FDG related images. Although PiB and FDG appeared to be similar, the PiB presented higher discrimination power in the very early cases with 82.76% sensitivity and 83.3% specificity. López et al. [10] used PCA and linear discriminant analysis (LDA)/-fisher discriminant ratio (FDR) for the feature selection process in a CAD system and applied artificial neural network (ANN)/SVM for classification, leading to a classification accuracy of 89.52%. Martínez-Murcia et al. [11] presented a three stage CAD system where the Mann-Whitney-Wilcoxon U-Test was utilized for voxel selection to prevent selecting outliers, factor analysis for feature extraction, and linear SVM for classification. This system was reported to have an accuracy of 92.9% with PET scans. Chaves et al. [12-15] exploited the association rule (AR) mining to develop a CAD system for the early diagnosis of AD. The system was tested on two data sets, including PET scans, achieving an accuracy of 92%. Padilla et al. [16] reported a CAD system that combined a nonnegative matrix factorization (NMF) for feature selection and reduction, and a SVM with confidence bounds for classification, resulting in a classification accuracy of 86%.

Even though many studies utilized ^{11}C PiB–PET scans to uncover the ambiguity of AD, these studies only produced global diagnosis. However, global diagnosis are not always adequate, especially when considering the intra-patient variation in abnormalities and the treatment procedures (i.e. personalized

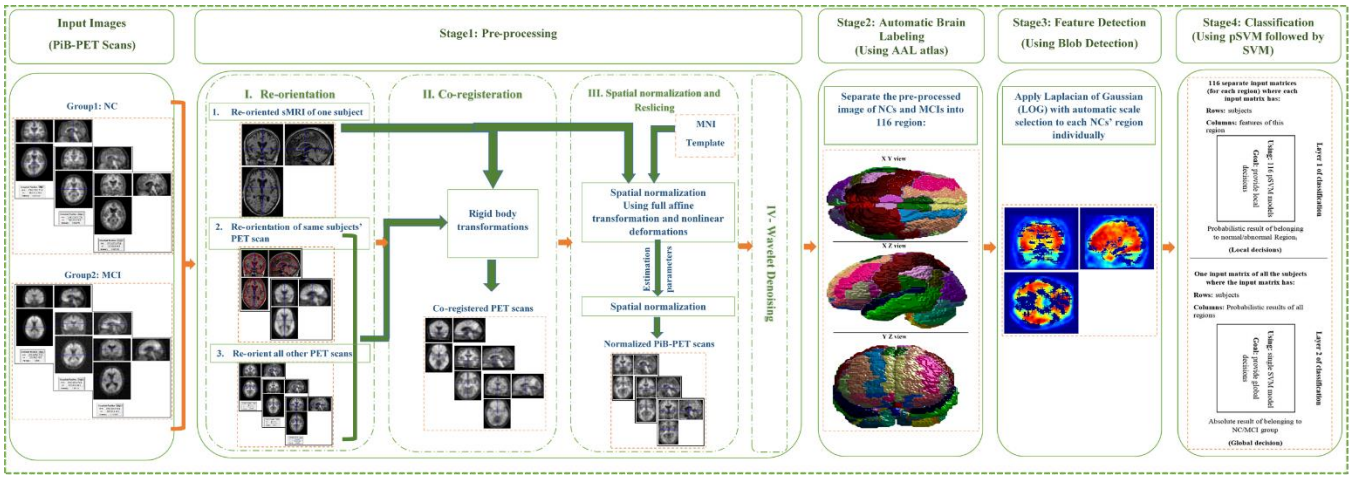

Figure 1: The framework of the proposed local and global based CAD system.

medicine). Thus, local diagnosis need to be incorporated with global diagnosis for accurate discovery due to disease related ambiguity.

To overcome these limitations, this manuscript presents a comprehensive CAD system to assist in the early diagnosis of AD with two distinct advantages over previous work: (1) the proposed system was trained on features extracted per Automated Anatomical Labeling (AAL) atlas based regions of the brain to improve diagnostic performance; (2) the proposed system produces an AAL region-local diagnosis that detects pathology for each brain region in addition to the overall diagnosis. The proposed CAD system enables early diagnosis, personalized medicine, and extensive analysis of disease ambiguities. The CAD system utilizes the AAL atlas [17] as it provides regional information within 116 brain regions, including 90 cerebral regions (45 regions in each hemisphere) and 26 regions in the cerebella (9 regions in each hemisphere of the cerebellar and 8 regions in the vermis). AAL was selected as it provides detailed regional information, and as it has been recommended to be used with PET scans [18].

2. METHODS

This paper introduces a comprehensive CAD system to assist in the early diagnosis of AD through providing local as well as global diagnosis. Fig. 1 illustrates the processing pipeline of the proposed framework, which consists of four main stages: preprocessing, automatic brain labeling, feature extraction, and diagnosis/classification stages. In the preprocessing stage, the images are re-oriented, co-registered and spatially normalized. This is followed by partitioning the brain into separate regions using the AAL atlas. Then, for each region, blob detection using the scale-invariant Laplacian of Gaussian (LoG) is applied to identify the significant brain regions with high Aβ plaques. Finally, two classification layers were built. In the first layer, 116 separate probabilistic SVM (pSVM) models were trained for each region with the assistance of a posterior probability to generate a region based diagnosis. Then, a single SVM model, which concatenates all of the previously obtained probabilistic results for each subject, was built to obtain a final global diagnosis. The details of the proposed framework are discussed in the following subsections.

2.1. Preprocessing

For the preparation of this paper, ^{11}C PiB-PET scans, which were collected from the Alzheimer's Disease Neuroimaging Initiative (ADNI) database (www.loni.ucla.edu/ADNI), were used. The database contains scans of normal control (NC) and mild cognitive impairment (MCI) subjects. These scans are co-registered, averaged, spatially oriented, intensity normalized, and smoothed through ADNI preprocessing operations [19]. In the proposed framework, the preprocessing operations aim to achieve two main goals, which are data standardization and de-noising. The first goal was reached using four operations: re-orientation, co-registration, spatial normalization, and re-slicing. Then, a wavelet based denoising operation was performed to meet the second goal.

For the standardization goal, the ADNI-processed scans were re-oriented to the AC-PC line that was different from the ADNI-built-in re-orientation operation. In ADNI, the scans were re-oriented into a standard image grid that, in turn, orients the subject's anterior-posterior axis to be parallel to the AC-PC line. Here, the data re-orientation operation is performed in three essential steps. First, one of the test subjects is selected, and its sMRI is re-oriented to the AC-PC line. Second, the associated ^{11}C PiB-PET scan of the chosen subject was re-oriented to the re-oriented sMRI scan producing a re-orientation matrix. Finally, the re-orientation matrix is applied to the other ^{11}C PiB-PET scans.

After AC-PC line based re-orientation, the ^{11}C PiB-PET scans were co-registered to the previously used sMRI scan as a preparation for the spatial normalization process. This co-registration was performed through rigid body transformations (i.e. translations and rotations) by the mutual information cost function.

Then, the spatial normalization and re-slicing were applied to standardize the scans to the Montreal Neurological Institute (MNI)-space. This standardization serves the automatic brain labeling step of the framework where the AAL atlas provides an anatomical parcellation of the MNI-space MRI-single-subject volume [17]. Therefore, the previously chosen sMRI scan was spatially normalized to the MNI template. This normalization used full affine transformation (i.e. translations, rotations, zooms, and shears) in addition to the nonlinear deformations to achieve more precise results. Then, the resulting transformation function could be applied to spatially normalize the ^{11}C PiB-PET scans since they were previously co-registered with the spatially normalized sMRI scan.

After data standardization, wavelet based denoising was applied to retain the quality while freeing the scans from the noise that may have been produced during the acquisition and/or the transmission [20]. Wavelets are used due to their popularity in the context of medical denoising and enhancement because of their good localization properties [21]. The following procedure to achieve this

idea goes through three stages. First, the forward transformation of the image is performed by using the suitable mother wavelet, scale, and levels of decomposition. Second, the estimated threshold is used to select the shrinkage rule (alternatively known as thresholding) and to apply it to the detail coefficients [22, 23]. Finally, the inverse transformation is performed on the modified coefficients to obtain the denoised image [24]. Further details about the thresholding rule and a comparative analysis of denoising process based on Discrete Wavelet Transforms (DWTs) can be found in [21]. In this paper, the symlet8 mother wavelet was chosen along with Stein's Unbiased Risk Estimate as a threshold selection rule and soft thresholding as in [25]. The choice of symlet8 was due to the fact that in general symlets mother wavelet is a compact support orthogonal mother wavelet with both the least asymmetry and the highest number of vanishing moments for a given support width. In turn, these properties could help in locally preserving the spatial image's characteristics [26].

2.2. Automatic brain labeling

The ultimate goal of the proposed system is to reveal the healthy or pathological status of each region of the brain, which will assist in early diagnosis and treatment of AD. The regions of the brain have been separated into 116 regions using the AAL brain atlas. Each voxel location in an image corresponding to brain tissue was mapped to one of the 116 regions of this atlas.

2.3. Feature extraction using blob detection

Each of the 116 regions is separately fed in this step for the purpose of feature extraction. Mainly, the blob detection aims to highlight the circular structures (i.e., blobs) from the images as a feature. The blob itself is either a local minimum or maximum of a radially symmetric distribution of the intensity [27]. For blob detection, there are two cases. If the blob's characteristics are known (e.g. size), the LoG filter is massively applied with a certain standard deviation (σ), which is chosen based on the blob size as follows [28]:

$$LoG(x,y) = -\frac{1}{\pi\sigma^2}\left(1-\frac{x^2+y^2}{\sigma^2}\right)exp\left(-\frac{x^2+y^2}{\sigma^2}\right)$$

where x and y are the region's coordinates. On the contrary, if the blob size and scale are unknown, the LoG filter could be applied with σ to be used as a parameter of the LoG equation producing scale-invariant blob detection [28]. At the end of this step, blob features of each of the 116 brain regions are extracted for each input scan. These features are subsequently supplied as an input for the upcoming classification step.

2.4. Diagnosis/Classification

For the diagnosis/classification process, the SVM classifier was used to produce a generalization model that can help obtain a correct prediction for new data [29]. In this paper, besides using SVM, pSVM was utilized to produce a posterior probability output for each region to belong to the normal/abnormal class. Therefore, the classification step goes into two subsequent layers. First, 116 separate pSVM models were constructed using the features of all subjects' regions, NCs and MCIs, as inputs. These regions based probabilistic results (local results) helps in making more detailed diagnosis. Then, a concatenation of all the regional based probabilistic results for each subject is fed to the second SVM layer with only one SVM model to be constructed. This layer provides a global subject based result.

3. EXPERIMENTAL RESULTS

A set of ^{11}C PiB-PET scans, which were obtained from the ADNI database, were used to evaluate the proposed framework. The used data set contains a total number of 84 scans. These scans are obtained from 19 NC and 65 MCI subjects. It is important to mention here that SPM12 [30] and xjview [31], which are MATLAB toolboxes, were utilized to build the proposed framework.

Two experimental results are presented as follow. The first result illustrates the meaning of the extracted features. Then, the second result shows three classification related results: a comparison of the SVM-related kernels (regarding the two layers), samples of the obtained local based results and finally, a comparison of the proposed system with related studies that use the same database. Note that, in the final comparison, the results of the related work are obtained through their implementation of their systems.

Regarding the features, the system extracts regionally based features (blobs) vectors with dimensions vary according to the detected local minimum or maximum radially symmetric intensity distribution in each region. Fig. 2 shows a sample of the blob detection of NC and MCI subjects. The blobs are detected, including the reveal of the abnormal parts from the input scans.

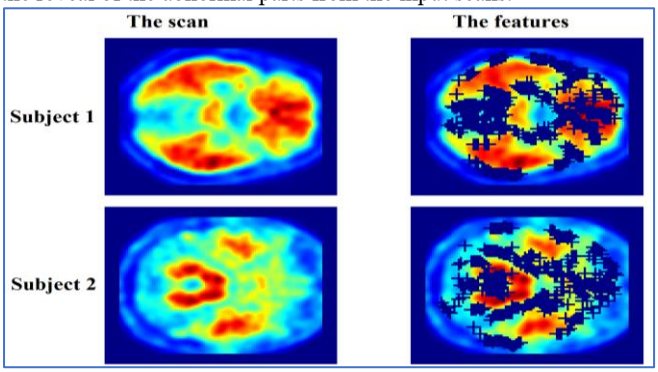

Figure 2: Demonstration of the extracted features represented as blue pulses for two different subjects.

For the classification results, first, three SVM kernels were compared, namely polynomial, radial basis function (RBF), and linear kernels. For SVM optimization, the features were standardized through centering and scaling them using their weighted mean and standard deviation. Table 1 shows the effect of the choice of the kernel on the SVM classification accuracy (Acc.), specificity (Spec.) and sensitivity (Sens.) as percentages. These results were obtained using both k-fold, with k=4, and leave-one-subject-out cross verification methods where the used dataset was partitioned into training and testing data. Regarding the local diagnosis, the classifier achieved a maximum of 77.38%, 100% and 50.41% in accuracy, sensitivity, and specificity, respectively.

As an example of personalized diagnosis, the reconstructed cortices of two individuals are presented in Fig. 3. The AAL brain regions identified by the proposed system as abnormal are highlighted. This visualization can assist experts in deciding the appropriate intervention given the location and severity of the pathology. Comparing the results of our methodology to other methods tested on the same data set (Table 2) clarify the advantages of the proposed system.

Table 1: Comparison of SVM performance with various kernels.

	Layer2 / Layer 1	Polynomial	RBF	Linear
K fold cross validation using K=4	Polynomial	Acc.:81.27 Spec.:19.65 Sens.:98.21	Acc.: 22.52 Spec.: 100 Sens.: 0	Acc.:76.58 Spec.: 0 Sens.:100
	RBF	Acc.:77.48 Spec.: 0 Sens.:100	Acc.: 76.58 Spec.: 0 Sens.:100	Acc.:77.29 Spec.: 0 Sens.:100
	Linear	Acc.:89.49 Spec.:53.63 Sens.:100	Acc.:22.71 Spec.:100 Sens.:0	Acc.:77.29 Spec.:100 Sens.:0
Leave-one-subject-out cross validation	Polynomial	Acc.:82.14 Spec.:31.57 Sens.:96.92	Acc.: 23.80 Spec.: 100 Sens.: 1.53	Acc.: 77.38 Spec.: 0 Sens.:100
	RBF	Acc.:100 Spec.:100 Sens.:100	Acc.: 83.33 Spec.: 73.68 Sens.:100	Acc.:100 Spec.:100 Sens.:100
	Linear	Acc.:89.28 Spec.:52.63 Sens.:100	Acc.: 22.61 Spec.: 100 Sens.: 0	Acc.: 77.38 Spec.: 0 Sens.:100

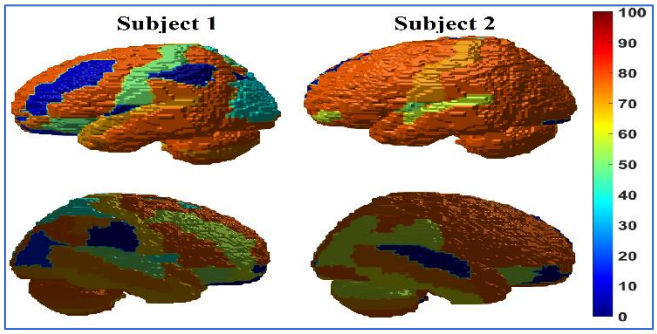

Figure 3: Two different subjects showing local diagnosis with their associated percentages represented by the color-bars.

Table 2: The performance of the proposed system in relation to other related work using leave-one-subject-out cross-validation.

	Chaves et al. [15]	The proposed system
Acc.	90.48	100
Spec.	100	100
Sens.	87.69	100

4. DISCUSSION

The scale invariant LoG was able to detect the local minimum/maximum radial symmetric distribution of intensity, Fig. 1. This may enable detection of abnormalities as AD has been reported to have significant retention of PIB in the brain regions that have increased Aβ plaques [28]. With regard to the classification results, the RBF kernel for the pSVM with both linear and polynomial kernels for the SVM gave a maximum result of 100% accuracy using leave-one-subject-out verification method, Table 1. On the other hand, the k-fold, with k=4, achieved a maximum accuracy of 89.49%. In general, achieving these levels of accuracy demonstrate the ability of the proposed system for early detection of AD. In addition, the obtained results reveal that increasing the size of the training data enhances the overall accuracy of the diagnosis. Finally, the proposed CAD system has a higher accuracy compared to previously published CAD systems and demonstrates the efficacy of using the blob detection method along with the SVM classifier in distinguishing between NC and MCI subjects.

5. CONCLUSION

The early diagnosis of AD challenging due to pre-clinical appearance of the pathological features, and the intra-patient variability of the effect of AD. Among diagnostic tests, PiB-PET scans show a significant role by identifying the Aβ abnormalities for early diagnosis. This manuscript proposes a CAD system that stratifies and presents both local and global diagnosis. Local diagnosis are for individual regions of the brain that were labeled/partitioned using the AAL atlas and addressed in the first classification stage using the pSVM classifier. The local diagnosis enables early disease identification despite intra-patient variability and may consequently facilitate personalized medicine. The proposed system also provides a global diagnosis of whether the subject is considered NC or mildly impaired through the SVM classifier. To present this system, the discriminant features have been obtained through blob detection in an attempt to differentiate between the characteristics of the NC and the MCI groups. The proposed system is demonstrated to have a maximum classification accuracy, sensitivity, and specificity of 100% for global diagnosis and is superior to previously related work in literature. Our future work will focus on improving the accuracy of the local diagnosis in addition to performing double-blind clinical trials.

6. REFERENCES

[1] "World Health Organization", World Health Organization, 2016. [Online]. Available: http://www.who.int/. [Accessed: 07- Nov- 2016].

[2] D. Brown, Brain diseases, and metalloproteins, Boca Raton, FL, Pan Stanford Pub., 2012.

[3] J. Hodler, et al., Diseases of the brain, head & neck, spine, 2012-2015, Milan, Springer, 2012.

[4] N. Ali, Understanding Alzheimer's, Lanham, Md., Rowman & Littlefield Publishers, 2012.

[5] L. Scinto and K. Daffner, Early diagnosis of Alzheimer's disease. Totowa, N.J.: Humana Press, 2000.

[6] B. Davis, Alzheimer talk, text, and context, 1st ed. New York: Palgrave Macmillan, 2005.

[7] C. Jack, et al., "Hypothetical model of dynamic biomarkers of the Alzheimer's pathological cascade," The Lancet Neurology, vol. 9, no. 1, pp. 119-128, 2010.

[8] K. Johnson, et al., "Appropriate use criteria for amyloid PET: A report of the Amyloid Imaging Task Force, the Society of Nuclear Medicine and Molecular Imaging, and the Alzheimer's Association", Alzheimer's & Dementia, vol. 9, no. 1, pp. E1-E16, 2013.

[9] I. Illan, et al., "Machine learning for very early Alzheimer's Disease diagnosis; a 18F-FDG and PiB PET comparison", IEEE Nuclear Science Symposium & Medical Imaging Conference, pp. 2334 – 2337, 2010.

[10] M. López, et al., "Principal component analysis-based techniques and supervised classification schemes for the early detection of Alzheimer's disease," Neurocomputing, vol. 74, no. 8, pp. 1260-1271, 2011.

[11] F. Martínez-Murcia, et al., "Computer Aided Diagnosis tool for Alzheimer's Disease based on Mann–Whitney–Wilcoxon U-

Test," Expert Systems with Applications, vol. 39, no. 10, pp. 9676-9685, 2012.
[12] R. Chaves, et al., "Functional brain image classification using association rules defined over discriminant regions," Pattern Recognition Letters, vol. 33, no. 12, pp. 1666-1672, 2012.
[13] R. Chaves, et al., "Association rule-based feature selection method for Alzheimer's disease diagnosis," Expert Systems with Applications, vol. 39, no. 14, pp. 11766-11774, 2012.
[14] R. Chaves, et al., "Integrating discretization and association rule-based classification for Alzheimer's disease diagnosis," Expert Systems with Applications, vol. 40, no. 5, pp. 1571-1578, 2013.
[15] R. Chaves, et al., "FDG and PIB biomarker PET analysis for the Alzheimer's disease detection using Association Rules," 2012 IEEE Nuclear Science Symposium and Medical Imaging Conference Record (NSS/MIC), pp. 2576-2579, 2012.
[16] P. Padilla, et al., "NMF-SVM Based CAD Tool Applied to Functional Brain Images for the Diagnosis of Alzheimer's Disease," IEEE Transactions on Medical Imaging, vol. 31, no. 2, pp. 207-216, 2012.
[17] N. Tzourio-Mazoyer, et al., "Automated Anatomical Labeling of Activations in SPM Using a Macroscopic Anatomical Parcellation of the MNI MRI Single-Subject Brain," *NeuroImage*, vol. 15, no. 1, pp. 273-289, 2002.
[18] K. Ota, et al., "Effects of imaging modalities, brain atlases and feature selection on prediction of Alzheimer's disease," Journal of Neuroscience Methods, vol. 256, pp. 168-183, 2015.
[19] "ADNI | Alzheimer's Disease Neuroimaging Initiative", Adni.loni.usc.edu, 2016. [Online]. Available: http://adni.loni.usc.edu/. [Accessed: 07- Nov- 2016].
[20] S. Agrawal and Y. Bahendwar, "Denoising of MRI images using thresholding technique through wavelet transform," International Journal of Computer Applications in Engineering Science, vol. 1, no. 3, pp. 361–364, 2011.
[21] Y. Bahendwar and G. Sinha, "A Comparative Performance Analysis of Discrete Wavelet Transforms for Denoising of Medical Images", Lecture Notes in Mechanical Engineering, pp. 417-424, 2016.
[22] C. Taswell, "The what, how, and why of wavelet shrinkage denoising," Computing in Science & Engineering, vol. 2, no. 3, pp. 12-19, 2000.
[23] B.-J. Yoon and P. Vaidyanathan, "Wavelet-based denoising by customized thresholding", 2004 IEEE International Conference on Acoustics, Speech, and Signal Processing, vol. 2, pp. ii-925-8, 2004.
[24] Y. Bahendwar and G. Sinha, "A modified algorithm for denoising MRI images of lungs using discrete wavelet transform," in National Conference on Innovative Paradigms in Engineering & Technology (NCIPET-2012), pp. 29–32, 2012.
[25] U. Bagci and D. Mollura, "Denoising PET Images Using Singular Value Thresholding and Stein's Unbiased Risk Estimate", in Medical image computing and computer-assisted intervention: MICCAI. International Conference on Medical Image Computing and Computer-Assisted Intervention, pp. 115-122, 2013.
[26] M. Vallières, et al., "A radiomics model from joint FDG-PET and MRI texture features for the prediction of lung metastases in soft-tissue sarcomas of the extremities," Physics in Medicine and Biology, vol. 60, no. 14, pp. 5471-5496, 2015.
[27] K. Toennies, Guide to medical image analysis, 1st ed. London: Springer, 2012.
[28] J. Shin, et al., "Voxel-based analysis of Alzheimer's disease PET imaging using a triplet of radiotracers: PIB, FDDNP, and FDG," NeuroImage, vol. 52, no. 2, pp. 488-496, 2010.
[29] C. Campbell and Y. Ying, Learning with support vector machines, 1st ed. [San Rafael, Calif.]: Morgan & Claypool, 2011.
[30] W. NeuroImaging, "SPM12 - Statistical Parametric Mapping", Fil.ion.ucl.ac.uk, 2016. [Online]. Available: http://www.fil.ion.ucl.ac.uk/spm/software/spm12/. [Accessed: 07- Nov- 2016].
[31] "xjView | A viewing program for SPM", Alivelearn.net, 2017. [Online]. Available: http://www.alivelearn.net/xjview. [Accessed: 23- Jan- 2017].
[32] J. Jiang, et al., "A Computed Aided Diagnosis tool for Alzheimer's disease based on 11C-PiB PET imaging technique," 2015 IEEE International Conference on Information and Automation, 2015.